Article

Temperature-Stable Energy Storage Properties of Tungsten Bronze Type Compounds

Xi Shi[1]* and Neamul H Khansur[1]*

[1]Department of Materials Science and Engineering, Friedrich-Alexander-University Erlangen-Nürnberg (FAU), Erlangen, Germany

* Correspondence: to whom correspondence should be addressed: xi.shi@fau.de; neamul.khansur@fau.de

Abstract: The temperature-dependent energy storage properties of four tungsten bronze phase compounds are studied together with an investigation of their structure and temperature-dependent permittivity response, *i.e.*, $Ba_6Ti_2Nb_8O_{30}$ (BTN), $Ba_6Zr_2Nb_8O_{30}$ (BZN), $Sr_3TiNb_4O_{15}$ (STN) and $Sr_3ZrNb_4O_{15}$ (SZN) ceramics. It was found that BZN has smaller grains and a more porous structure than BTN. SZN shows no clear grain boundaries with the most porous structure among all samples, exhibiting a much lower permittivity response than other samples with no signs of phase transitions from room temperature to 400 °C. Though the energy storage response of those samples is generally quite low, it exhibits a rather good temperature stability. It was suggested that by obtaining a denser structure through chemical modification or other methods, those tungsten bronze ceramics with good temperature stability could be promising as energy storage devices when improved energy storage properties are achieved.

Introduction

Dielectric ceramic capacitors show high power density (~ 10^8 w/kg), fast charge-discharging rate (<1 μs), and good thermal stability, therefore are crucial as energy storage devices in applications such as pulse power industries, medical equipment, and electronic devices [1], *etc*. Among those dielectric ceramic capacitors, relaxor ferroelectrics show better energy storage properties (such as recoverable energy storage density, W_{rec}, and energy efficiency, η) than ferroelectrics and paraelectric materials due to the higher maximum polarization, lower energy loss, and higher breakdown field attributed from their unique microstructure with polar nano regions [1]. The typical material systems include $PbZrO_3$-based and lead-free perovskite-structured systems including $BaTiO_3$ (BT)-based, $K_{0.5}Na_{0.5}NbO_3$ (KNN)-based, and $Na_{1/2}Bi_{1/2}TiO_3$ (NBT)-based ceramics. Since the usage of lead is restricted due to its toxicity to the environment, research is intensively focused on developing promising lead-free systems, and great research advances have been achieved. For example, a high W_{rec} of 1.76 J/cm^3 was reported in $0.94Bi_{0.55}Na_{0.45}TiO_3$-$0.06BaTiO_3$ ceramics under 75 kV/cm [2], BT based $0.7BT$-$0.3BiScO_3$ ceramics obtained a W_{rec} of 2.3 J/cm^3 under 225 kV/cm [3], 0.85KNN-0.15ST showed a W_{rec} of 4.03 J/cm^3 under a field of 400 kV/cm [4].

Tetragonal tungsten bronze (TTB) structure with polar distortion is one of the major categories of lead-free ferroelectrics [5-8]. Over the recent years, TTB ferroelectrics have been researched due to their excellent non-linear optic, pyroelectric, and optoelectronic properties [9, 10]. In the meantime, tetragonal tungsten bronze (TTB) structured materials could also be potential energy storage materials, such as $Sr_{1-x}Ba_xNb_2O_6$ (SBN), $Ba_{6-3x}Nd_{8+2x}Ti_{18}O_{54}$ (BNT), $Ba_6Ti_2Nb_8O_{30}$ (BTN), $Sr_3TiNb_4O_{15}$ (STN). They have a general formula $(A1)_2(A2)_4(C)_4(B1)_2(B2)_8O_{30}$. A1 represents a 12-coordinate site, A2 is a 15-coordinate site, and B1 and B2 are 6-coordinate octahedral sites [11]. Smaller triangular (C) sites could be (partially) filled by small low-charged cations which are generally empty, therefore the formula becomes $A_6B_{10}O_{30}$. TTB materials are normally porous due to the abnormal grain growth during sintering [12] and the properties would greatly vary when different elements are located at A, B, and C sites, allowing the manipulation of their

 doi:10.20944/preprints202306.1050.v1

structure and properties [13]. TTB ceramics with a relaxor ferroelectric nature are especially attractive as energy storage devices. For example, Fe-doped tungsten bronze $Sr_{1-x}Ba_xNb_2O_6$ (SBN) ceramics could achieve W_{rec} of 0.68 J/cm^3 and η of 83.6 % [14]. MgO-$Sr_{0.7}Ba_{0.3}Nb_2O_6$ composites show W_{rec} of 0.93 J/cm^3 together with η of 89.4 %. The $(Sr_{0.7}Ba_{0.3})_5LaNb_7Ti_3O_{30}$ tungsten bronze ceramic was reported to have a W_{rec} of 1.36 J/cm^3 and η of 91.9 % [6].

$Ba_6Ti_2Nb_8O_{30}$ (BTN) ceramic was first reported in 1965 [15]. It has a tetragonal structure (space group *P4bm*), with lattice parameters a = b = 12.53 Å and c = 4.01 Å. The structure consists of NbO_6 octahedra sharing corners occupied by Nb and Ti forming two main interstices (A1 and A2) [16]. Both pentagonal A1-sites and tetragonal A2-sites are predominantly occupied by Ba. The co-existence of pentagonal and tetragonal sites results in trigonal vacant C-sites [16]. BTN ceramic was initially studied as a ferroelectric due to its low dielectric loss and low-temperature coefficient of relative permittivity [17, 18]. It was reported that its electrical properties are preferable when sintering in a reducing atmosphere leading to more electrons generated together with oxygen vacancies [19]. $Sr_3TiNb_4O_{15}$ (STN) tungsten bronze phase has been recently determined to have an orthorhombic structure with unit cell a = 12.363 Å, b = 12.4 Å, and c = 7.76 Å [11, 20], different from BTN. It is suggested the smaller ionic radius of Sr^{2+} compared to Ba^{2+} allows for more flexibility in the structure leading to this orthorhombic structure [21]. Pure STN is known to show low conductivity and owns a relaxor nature due to the composition disorder at A and B sites with Curie temperature at around 600 °C [22]. Unfortunately, there is a lack of fundamental understanding of those materials as well as their performance as potential energy storage devices.

In this work, we have looked into the structural features and small signal dielectric properties of four representative tungsten bronze compounds, *i.e.*, $Ba_6Ti_2Nb_8O_{30}$ (BTN), $Ba_6Zr_2Nb_8O_{30}$ (BZN), $Sr_3TiNb_4O_{15}$ (STN), $Sr_3ZrNb_4O_{15}$ (SZN) ceramics as well as systematically studied their energy storage properties at different temperatures, which could provide insights for implementing them as temperature stable energy storage devices, provided with improved energy storage response.

Methodology

$Ba_6Ti_2Nb_8O_{30}$ (BTN), $Ba_6Zr_2Nb_8O_{30}$ (BZN), $Sr_3TiNb_4O_{15}$ (STN), $Sr_3ZrNb_4O_{15}$ (SZN) tungsten bronze ceramics were fabricated using the conventional solid-state reaction method using high-purity reagent powders in stoichiometric ratios: $BaCO_3$ (Sigma Aldrich, 99.9 %), TiO_2 (Sigma Aldrich, 99.9 %), Nb_2O_5 (Sigma Aldrich, 99.99 %), $SrCO_3$ (Sigma Aldrich, 99.9 %) and ZrO_2 (Sigma Aldrich, 99 %). The mixed powders for each composition were milled for 24 h in ethanol and calcined at 950 °C in air for 42 hours. After the second milling, the powders were pressed into green bodies and were further densified using a cold isostatic press. Sintering of pellet-shaped samples was done at 1300 °C for a total of 7 days in air.

X-ray diffraction (XRD) patterns were collected from the ground sample surfaces using a Bruker D8 Advance diffractometer (Bruker AXS GmbH, Germany). The microstructure of all sintered samples was examined under a scanning electron microscope (SEM) (Quanta 200, FEI Co., USA). The relative permittivity was measured with an LCR meter (E4980AL, Keysight, USA) from room temperature to 400 °C with 2 K/min heating/cooling rate on samples with Pt electrodes (Balzers SCD040) on both sides. The energy storage property test at different temperatures was based on measuring the polarization-electric field (PE) loops of ground samples (around 0.5 mm thick). Before measurement, the ground samples are annealed in air at 500 °C for 1 hour to remove the stress effects from mechanical processing and then sputtered with Pt electrodes. The tests are performed using a unipolar waveform under a frequency of 100 Hz with a maximum field of 140 kV/cm on a TF Analyser 2000 (aixACCT (aixPES), Aachen, Germany). Samples were immersed in insulating silicon oil (Wacker®-AP 100 Silicone Fluid) during the tests.

Preprints (www.preprints.org) | NOT PEER-REVIEWED | Posted: 14 June 2023 doi:10.20944/preprints202306.1050.v1

Results and Discussion

The X-ray diffraction (XRD) patterns shown in **Error! Reference source not found.** indicate that both BTN ($Ba_6Ti_2Nb_8O_{30}$) [16] and BZN ($Ba_6Zr_2Nb_8O_{30}$) [13] have a tetragonal structure with the space group *P4bm*. For the XRD pattern belonging to BTN ($Ba_6Ti_2Nb_8O_{30}$), the strongest peak at 2θ = 31.77° (see the star label in Fig.1b) and peaks at 2θ = 29°, 43° correspond to a secondary phase $Ba_5Nb_4O_{15}$, based on a previous study on BTN using Rietveld structural refinement method [19]. The peaks at 2θ = 25.5° correspond to another secondary phase $Ba_3Ti_4Nb_4O_{21}$. $Ba_6Zr_2Nb_8O_{30}$ (BZN) has the same structure as BTN and is also a relaxor ferroelectric with the equal-valence B-site substitution of Zr^{4+} for Ti^{4+} [13]. For BZN, the strongest peak located at 2θ = 31.6° also corresponds to $Ba_5Nb_4O_{15}$, same as BTN (see the labeled peaks in Fig. 1b), of which the location of the peak is a bit right-shifted compared to an earlier work [13]. As the $Sr_3Ti_{1-x}Zr_xNb_4O_{15}$ (STZN) compound, the Ti-rich end member $Sr_3TiNb_4O_{15}$ (STN) (x = 0.0) has the orthorhombic structure with $Pna2_1$ symmetry [11]. For STN, the peaks at 2θ = 23°, 46° and the highest peak located at 2θ = 32.5° (see the labelled peaks in Fig.1b) correspond to a secondary phase $Sr(Ti_{0.5}Nb_{0.5})O_3$ with cubic perovskite structure ($Pm\bar{3}m$), the peaks at 2θ = 26°, 35° corresponds to another secondary phase $Ti_{0.67}Nb_{0.33}O_2$ [23]. The $Sr_3ZrNb_4O_{15}$ (S**Error! Reference source not found.**ZN) end member (x = 1.0) has the same crystal symmetry as STN despite being substituted with larger cations of Zr^{4+} (radius 0.72 Å) instead of Ti^{4+} (radius 0.605 Å), consistent with the earlier study [11].

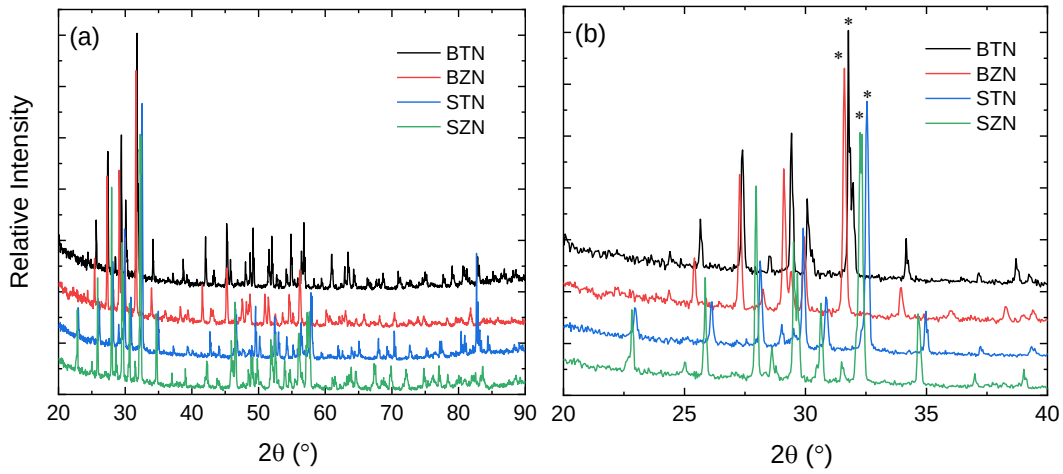

Figure 1. Normalized XRD patterns of BTN, BZN, STN and SZN at room temperature between 10° and 90° (a); enlarged 2θ range between 20° and 40° with the strongest peak marked with star labels (b).

Error! Reference source not found. shows the microstructure features of the surfaces of the as-sintered samples under SEM. It is seen that they all have a porous structure with different extents of porosity. In Fig. 2a, BTN shows uneven equiaxed grains with an average grain size of 10 μm, consistent with earlier studies [16]. Among the four samples, BZN has the smallest grains (size of around 1-2 μm) and an intergranular array of pores and grains (Fig. 2b), in agreement with a previous study [13]. Compared with other samples, STN has more round-shaped grains (around 5 μm in size) (Fig. 2c). As seen in Fig. 2d, SZN is quite porous with connected irregular grains and unclear grain boundaries [13], which could influence its permittivity response and energy storage properties. It is suggested the intensively distributed pores and unclear grain boundaries in those samples (especially in BZN and SZN) are due to the release of CO_2 gas during the sintering process, resulting in low sample density [13].

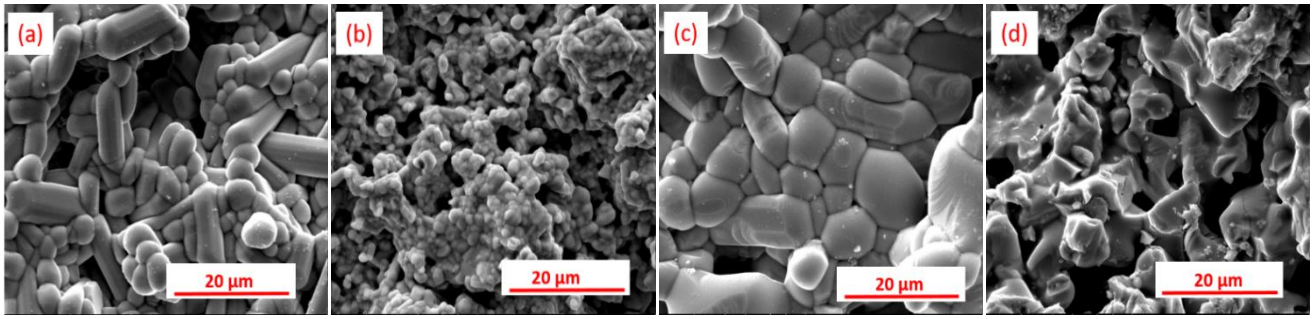

Figure 2. Microstructure image of (a) BTN; (b) BZN; (c) STN; and (d) SZN ceramic samples.

Error! Reference source not found. shows the temperature-dependent permittivity o f the four TTB samples. Except for SZN which has a rather low relative permittivity (< 150) which is probably associated with its porous structure (see Fig. 2d), the maximum permittivity of other samples is all above 1000.

The transition at around 200 °C in BTN and 150 °C for STN (See Figs. 3a and c) indicates ferroelectric to paraelectric transition across Curie temperature, in agreement with previous works [22, 24]. Also, it is noted that this transition is broadened, possibly arising from the order-disorder variations of TiO_6 and NbO_6 for BTN and STN [25]. It has been reported that the diffuse exponent, γ, of STN and BTN is 1.41, and 1.95 respectively (when $\gamma = 1$ fits the normal ferroelectric when $\gamma = 2$ fits the typical relaxor) [25]. This type of diffused ferroelectric nature was also seen in other TTB ceramics [26, 27]. It is also seen that the dielectric loss of BTN and STN show a sudden increase from 200-250 °C together with the corresponding permittivity. Based on similar studies it can be concluded the corresponding peaks are not signals of transitions [11, 25]. Instead, it could be due to the motion of charge carriers including oxygen vacancies which are thermally activated at higher temperatures, with higher conductivity for samples [28]. Also, the increased dielectric loss could arise from the reduced contribution of ferroelectric domain walls at high temperatures [29]. Nevertheless, all samples have a rather low dielectric loss (less than 0.4 at frequencies above 1 kHz) till 400 °C, showing great potential in electronic applications, *etc*.

In Fig. 3b, BZN seems to show the strongest relaxor behavior among all samples (see Fig. 3b), showing strong frequency dependence in permittivity and loss tan δ, where the permittivity peaks move to higher temperatures with increasing frequency. In a similar study for porous BZN, the maximum permittivity also occurs around room temperature with strong frequency dispersion and γ of reaches 1.87 [13]. Similar to BTN and SZN, the permittivity and dielectric loss of BZN significantly increase from 200 °C and then decline at 300 °C. The corresponding peak at 300 °C could be associated with the dynamics of polar nano regions in this relaxor composition [13] or space charge effects.

Interestingly, SZN shows stable permittivity and dielectric loss values with increasing temperature, indicating no phase or structural transitions in this range (Fig. 3d). SZN could be ferroelectric with small domains or only piezoelectric [11]. Another study [11] suggested that there is a phase transition for SZN at 500 °C. Compared with STN, the shift of phase transitions to higher temperatures in SZN leads to more stable piezoelectric properties in this wide temperature range [11].

 doi:10.20944/preprints202306.1050.v1

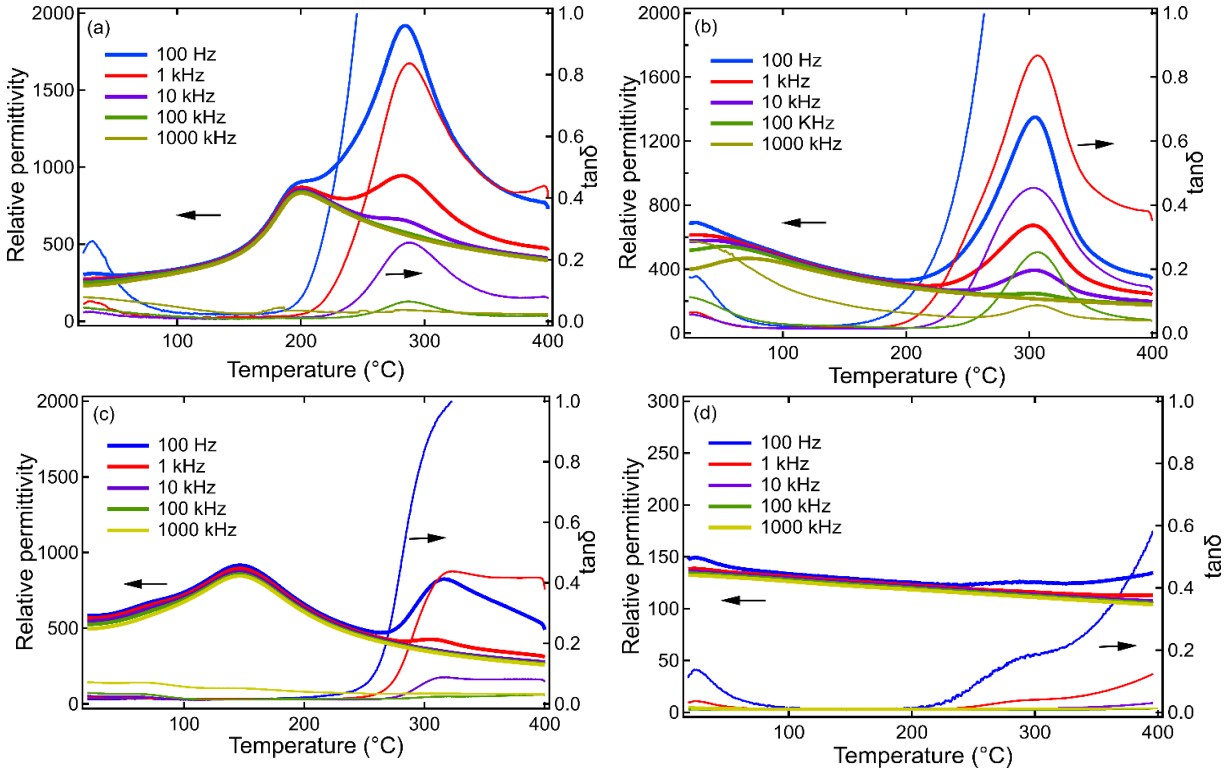

Figure 3. Temperature-dependent permittivity of BTN (a); BZN (b); STN (c) and SZN (d) (heating round) at different frequencies between room temperature and 400 °C.

Error! Reference source not found. a and b show the temperature-dependent P(E) l oops of BZN and STN samples under the maximum electric field of 140 kV/cm and 100 kV/cm, respectively. The maximum polarization (P_{max}) for BZN is below 6 μC/cm² under 140 kV/cm and below 8 μC/cm² for STN under 100 kV/cm. With temperature, the maximum polarization shows a slight decline for both samples. It is also found that the remanent polarization (P_r) gets larger and the P (E) loop becomes lossy at higher temperatures. The highest endurable electric field for BZN and STN samples is 140 and 120 kV/cm. BZN has a more porous structure than STN, as shown in **Error! Reference source not found.**. P ores would reduce the effective field applied on the sample, so the porous BZN can sustain a higher field [13] than STN with a denser microstructure. As seen in Fig. 4c, the W_{rec} for both samples is less than 1 μC/cm³, which is rather low to serve as energy storage materials. A similar energy storage response is also observed for the other two compositions, *i.e.*, BTN and SZN (the data for BTN and SZN are not shown due to lack of complete data at all temperatures). At room temperature, the W_{rec} of BZN at 140 KV/cm is 0.29 J/cm³ and shows a minor decline with temperature till 0.17 J/cm³ at 150 °C due to increased conductivity. In contrast, STN shows a similar W_{rec} at room temperature at 100 kV/cm with a slightly increased energy storage response at 150 °C of 0.29 J/cm³ due to reduced energy loss. The η (%) shows a similar trend as W_{rec} for both BZN and STN respectively. As seen in Fig. 4d, it declines significantly from around 80 % to 39 %, due to the increased conductivity with the sample with temperature for BZN, while for STN it overall increases from 70 % to 79 % from room temperature to 150 °C.

The porous structure of those TTB samples could lead to a low breakdown field and therefore limit their energy storage response, as shown in **Error! Reference source not f ound.**. Those energy storage properties could be potentially improved by chemical doping. For example, B site Ta-doped $Sr_2NaNb_{3.5}Ta_{1.5}O_{15}$ shows an increased breakdown strength and improved energy density of 3.99 J/cm³ and η of 91.7 % [30]. Sb-doped

Preprints (www.preprints.org) | NOT PEER-REVIEWED | Posted: 14 June 2023 doi:10.20944/preprints202306.1050.v1

$Sr_2Na_{0.8}Ag_{0.2}Nb_{4.7}Sb_{0.3}O_{15}$ tungsten bronze ceramics show enhanced relaxor nature and could achieve W_{rec} of 2.27 J/cm^3 and η of 93.3 % [31]. Those doped samples show dense microstructure and no abnormal growth crystal grains. Similar enhanced relaxor nature and energy storage properties are also seen in other ceramics such as Sb-modified $(Sr_{0.515}Ba_{0.47}Gd_{0.01})$ $(Nb_{1.9-x}Ta_{0.1}Sb_x)O_6$ (SBGNT-based) [32], CuO-modified $Sr_2NaNb_5O_{15}$-based [33] lead-free tungsten bronze relaxor ceramic, *etc*. Alternatively, sintering or post-annealing at a reducing atmosphere could also reduce the porosity and improved the electrical and energy storage properties [19].

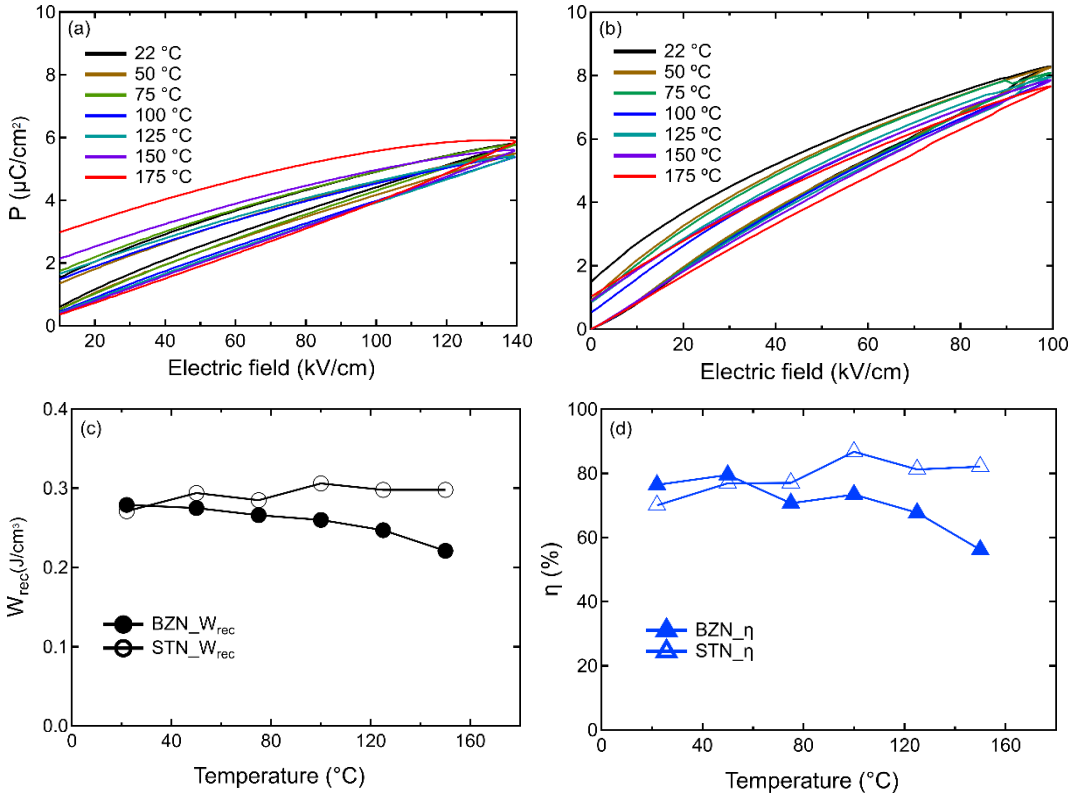

Figure 4. Temperature-dependent energy storage properties of BZN (a) and STN (b) from room temperature to 175 °C under field of 140 kV/cm and 100 kV/cm respectively; calculated recoverable energy density (W_{rec}) and energy storage efficiency (η) from room temperature to 150 °C for BZN (c) and STN (d).

Conclusions

The four compositions of tungsten bronze phase ceramics, *i.e.*, $Ba_6Ti_2Nb_8O_{30}$ (BTN), $Ba_6Zr_2Nb_8O_{30}$ (BZN), $Sr_3TiNb_4O_{15}$ (STN), $Sr_3ZrNb_4O_{15}$ (SZN) ceramics are systematically studied with a focus on their microstructure, dielectric response and its correlation with their temperature dependence of energy storage properties. Due to the different A and B site cations, those tungsten bronze ceramics show significantly different microstructure, permittivity response, and different extents of relaxor nature. Nevertheless, it was found that they generally have a low recoverable energy storage density (lower than 1 J/cm^3) due to their porous structure, especially SZN with an expected poorest energy storage response. Doping would be an ideal method to achieve a dense structure with smaller grains, enhanced relaxor nature, and promising energy storage properties.

Declaration of Competing Interest: The authors declare no competing interests that could influence the work in this paper.

Acknowledgments: X.S. and N.H.K. gratefully acknowledge the financial support for this work from the Deutsche Forschungsgemeinschaft under KH 471/2 and the ETI-funding of Friedrich-Alexander-University Erlangen-Nürnberg.

References

[1] X. Zhang, W. Ye, X. Bu, P. Zheng, L. Li, F. Wen, W. Bai, L. Zheng, Y. Zhang, Remarkable capacitive performance in novel tungsten bronze ceramics, J Dalton Transactions 50(1) (2021) 124-130.
[2] Q. Li, C. Zhou, J. Xu, L. Yang, X. Zhang, W. Zeng, C. Yuan, G. Chen, G. Rao, Tailoring antiferroelectricity with high energy-storage properties in Bi 0.5 Na 0.5 TiO 3–BaTiO 3 ceramics by modulating Bi/Na ratio, J Journal of Materials Science: Materials in Electronics 27 (2016) 10810-10815.
[3] H. Ogihara, C.A. Randall, S. Trolier-McKinstry, High-energy density capacitors utilizing 0.7 BaTiO3–0.3 BiScO3 ceramics, J Journal of the American Ceramic Society 92(8) (2009) 1719-1724.
[4] Z. Yang, H. Du, S. Qu, Y. Hou, H. Ma, J. Wang, J. Wang, X. Wei, Z. Xu, Significantly enhanced recoverable energy storage density in potassium–sodium niobate-based lead free ceramics, J Journal of materials chemistry A 4(36) (2016) 13778-13785.
[5] P. Jamieson, S. Abrahams, J.J.T.J.o.C.P. Bernstein, Ferroelectric tungsten bronze-type crystal structures. I. Barium Strontium niobate Ba0. 27Sr0. 75Nb2O5. 78, 48(11) (1968) 5048-5057.
[6] L. Cao, Y. Yuan, Z. Yang, E. Li, S. Zhang, Crystal structure, relaxor behaviors and energy storage performance of (Sr0. 7Ba0. 3) 5LaNb7Ti3O30 tungsten bronze ceramics, J Ceramics International 46(5) (2020) 6108-6114.
[7] M.-S. Kim, P. Wang, J.-H. Lee, J.-J. Kim, H.Y. Lee, S.-H. Cho, Site Occupancy and Dielectric Characteristics of Strontium Barium Niobate Ceramics: Sr/Ba Ratio Dependence, Japanese Journal of Applied Physics 41(Part 1, No. 11B) (2002) 7042-7047.
[8] S. Jindal, A. Vasishth, S. Devi, G.J.I.F. Anand, A review on tungsten bronze ferroelectric ceramics as electrically tunable devices, 186(1) (2018) 1-9.
[9] A. Simon, J. Ravez, Solid-state chemistry and non-linear properties of tetragonal tungsten bronzes materials, J Comptes Rendus Chimie 9(10) (2006) 1268-1276.
[10] B.-X. Wang, M. Krogstad, H. Zheng, R. Osborn, S. Rosenkranz, D.J.J.o.P.C.M. Phelan, Active and passive defects in tetragonal tungsten bronze relaxor ferroelectrics, 34(40) (2022) 405401.
[11] T.A. Whittle, T. Lu, P. Blanchard, J.R. Hester, Q. Gu, Y. Liu, S. Schmid, Synthesis, structure and dielectric properties of the Sr 3 Ti 1− x Zr x Nb 4 O 15,(0≤ x≤ 1), series of tungsten bronze type compounds, J CrystEngComm 22(30) (2020) 4994-5001.
[12] G.-h. Chen, B.J.J.o.a. Qi, compounds, Effect of CASP glass doping on sintering and dielectric properties of SBN ceramics, 473(1-2) (2009) 414-417.
[13] S.T. Zhang, G. Yuan, J. Chen, Z.B. Gu, B. Yang, J. Yin, W. Cao, Structural evolving sequence and porous Ba 6 Zr 2 Nb 8 O 30 ferroelectric ceramics with ultrahigh breakdown field and zero strain, J Journal of the American Ceramic Society 96(2) (2013) 555-560.
[14] H. Bai, J. Li, Y. Wu, Y. Hong, K. Shi, Z. Zhou, Exploring determinants of lattice structure and high energy storage properties of Fe-doped SBN ceramics, J Ceramics International 45(8) (2019) 11109-11113.
[15] N. Stephenson, The crystal structure of the tetragonal bronze, Ba6Ti2Nb8O30, J Acta Crystallographica 18(3) (1965) 496-501.
[16] D. Jiang, D. Ekren, F. Azough, S.J. Day, K. Chen, A. Mahajan, D.M. Kepaptsoglou, Q.M. Ramasse, M.J. Reece, R. Freer, The structure and thermoelectric properties of tungsten bronze Ba6Ti2Nb8O30, J Journal of Applied Physics 126(12) (2019) 125115.
[17] G. Roberts, R. Cava, W. Peck, J. Krajewski, Dielectric properties of barium titanium niobates, J Journal of materials research 12(2) (1997) 526-530.
[18] Y. Itoh, H. Iwasaki, Ferroelectric and optical properties of Ba6Ti2Nb8O30 single crystals, J Journal of Physics 34(10) (1973) 1639-1645.
[19] V. Massarotti, D. Capsoni, M. Bini, C. Azzoni, M. Mozzati, P. Galinetto, G. Chiodelli, Structural and spectroscopic properties of pure and doped Ba6Ti2Nb8O30 tungsten bronze, J The Journal of Physical Chemistry B 110(36) (2006) 17798-17805.
[20] Q. He, S. Schmid, X. Chen, B. Peng, C. Li, C. Hu, L. Liu, M.J.J.o.A.P. Hinterstein, Structure and relaxor ferroelectric behavior of the novel tungsten bronze type ceramic Sr5BiTi3Nb7O30, 131(16) (2022) 164102.
[21] E.O. Chi, A. Gandini, K.M. Ok, L. Zhang, P.S.J.C.o.m. Halasyamani, Syntheses, structures, second-harmonic generating, and ferroelectric properties of tungsten bronzes: A6M2M ‘8O30 (A= Sr2+, Ba2+, or Pb2+; M= Ti4+, Zr4+, or Hf4+; M ‘= Nb5+ or Ta5+), 16(19) (2004) 3616-3622.
[22] R. Neurgaonkar, J. Nelson, J. Oliver, Ferroelectric properties of the tungsten bronze M2+ 6M4+ 2Nb8O30 solid solution systems, J Materials research bulletin 27(6) (1992) 677-684.
[23] D. Jiang, Tungsten bronze structured compounds for thermoelectric applications, The University of Manchester (United Kingdom)2019.
[24] K.S. Rao, A. Subrahmanyam, P. Viswarupachary, Microstructural and anomalous resistivity behavior of modified ferroelectric Ba6Ti2Nb8O30, J Ferroelectrics 215(1) (1998) 95-102.
[25] Y. Yuan, X. Chen, Y.J.J.o.a.p. Wu, Diffused ferroelectrics of Ba 6 Ti 2 Nb 8 O 30 and Sr 6 Ti 2 Nb 8 O 30 with filled tungsten-bronze structure, 98(8) (2005) 084110.
[26] R.-J. Xie, Y. Akimune, K. Matsuo, T. Sugiyama, N. Hirosaki, T.J.A.P.L. Sekiya, Dielectric and ferroelectric properties of tetragonal tungsten bronze Sr 2− x Ca x NaNb 5 O 15 (x= 0.05–0.35) ceramics, 80(5) (2002) 835-837.

 doi:10.20944/preprints202306.1050.v1

[27] A. Bendahhou, P. Marchet, A. El-Houssaine, S. El Barkany, M. Abou-Salama, Relationship between structural and dielectric properties of Zn-substituted Ba5CaTi2−xZnxNb8O30 tetragonal tungsten bronze, CrystEngComm 23(1) (2021) 163-173.
[28] B. Parida, P.R. Das, R. Padhee, R.J.J.o.a. Choudhary, compounds, Phase transition and conduction mechanism of rare earth based tungsten-bronze compounds, 540 (2012) 267-274.
[29] P.R. Das, L. Biswal, B. Behera, R.J.M.R.B. Choudhary, Structural and electrical properties of Na2Pb2Eu2W2Ti4X4O30 (X= Nb, Ta) ferroelectric ceramics, 44(6) (2009) 1214-1218.
[30] X. Zhang, H. Wang, X. Bu, P. Zheng, L. Li, F. Wen, W. Bai, J. Zhang, L. Zheng, J. Zhai, Simultaneously Realizing Superior Energy Storage Properties and Outstanding Charge–Discharge Performances in Tungsten Bronze-Based Ceramic for Capacitor Applications, J Inorganic Chemistry 60(9) (2021) 6559-6568.
[31] S. Xu, R. Hao, Z. Peng, F. Zhang, D. Wu, P. Liang, X. Chao, L. Wei, Z. Yang, Relaxor nature and superior energy storage performance of Sr2Ag0. 2Na0. 8Nb5O15-based tungsten bronze ceramics through B-site substitution, J Chemical Engineering Journal 433 (2022) 133812.
[32] B. Yang, J. Zhang, X. Lou, Y. Gao, P. Shi, Y. Yang, M. Yang, J. Cui, L. Wei, S. Sun, Interfaces, Enhancing Comprehensive Energy Storage Properties in Tungsten Bronze Sr0. 53Ba0. 47Nb2O6-Based Lead-free Ceramics by B-Site Doping and Relaxor Tuning, J ACS Applied Materials 14(30) (2022) 34855-34866.
[33] S. Xu, R. Hao, Z. Yan, S. Hou, Z. Peng, D. Wu, P. Liang, X. Chao, L. Wei, Z. Yang, Enhanced energy storage properties and superior thermal stability in SNN-based tungsten bronze ceramics through substitution strategy, J Journal of the European Ceramic Society 42(6) (2022) 2781-2788.